Three-dimensional focus shaping of partially coherent circularly polarized vortex beams using a binary optic

2015 J. Opt. 17 065611

(http://iopscience.iop.org/2040-8986/17/6/065611)

IOP Publishing Journal of Optics
J. Opt. 17 (2015) 065611 (8pp) doi:10.1088/2040-8978/17/6/065611

Three-dimensional focus shaping of partially coherent circularly polarized vortex beams using a binary optic

Zhou Zhang[1,2], Hong Fan[3], Hua-Feng Xu[1,4], Jun Qu[5] and Wei Huang[1,2,4]

[1] Laboratory of Atmospheric Physico-Chemistry, Anhui Institute of Optics & Fine Mechanics, Chinese Academy of Sciences, Hefei, Anhui 230031, People's Republic of China
[2] Institute of Physics and Materials Science, Anhui University, Hefei, Anhui 230039, People's Republic of China
[3] School of Instrument Science and Opto-electronics Engineering, Hefei University of Technology, Hefei, Anhui 230009, People's Republic of China
[4] School of Environmental Science & Optoelectronic Technology, University of Science and Technology of China, Hefei, Anhui 230026, People's Republic of China
[5] Department of Physics, Anhui Normal University, Wuhu, Anhui 241000, People's Republic of China

E-mail: qujun70@mail.ahnu.edu.cn and huangwei6@ustc.edu.cn

Received 5 February 2015, revised 31 March 2015
Accepted for publication 14 April 2015
Published 27 May 2015

Abstract

The three-dimensional (3D) focus shaping technique using the combination of partially coherent circularly polarized vortex beams with a binary diffractive optical element (DOE) is reported. It is found that the intensity distribution near the focus can be tailored in three dimensions by appropriately adjusting the parameters of the incident beams, numerical aperture of the objective lens, and the design of the DOE. Numerical results show that partially coherent circularly polarized vortex beams can be used to generate several special beam patterns, such as optical chain, optical needle, optical dark channel, flat-topped field, and 3D optical cage. Furthermore, compared with the ordinary 3D optical cage, this kind of 3D optical cage generated by our method has a controllable switch; that is, it can be easy to 'open' and 'close' by controlling the coherence length of the incident beams. Our work may find valuable applications in optical tweezers, microscopes, laser processing, and so on.

Keywords: focus shaping, coherence, polarization, binary diffractive optical element, optical cage

1. Introduction

For a long time, there has been considerable research interest in light beam focusing and focus shaping techniques due to their wide applications, such as optical tweezers, microscopes, laser processing, etc [1–22]. It is well recognized that the tight focusing properties of beams can be modulated by using a binary diffractive optical element (DOE), such as polarization modulation [22, 23], amplitude modulation [24, 25], and phase modulation [26, 27]. Until now, much work has been made on the generation of some special beam patterns and their derivatives through a binary DOE. For example, Zhan *et al* generated the peak-centered, doughnut, and flat-topped focal intensity profiles by changing the polarization direction of cylindrical vector (CV) beams with a simple polarization rotator setup [23]. Wang *et al* demonstrated that an optical needle with a focal depth of 4λ, which consists of an almost pure longitudinal field, can be generated with the help of phase modulation [27]. Weng *et al* created the tunable multiple three-dimensional (3D) optical cage by using the CV beams with a specially designed DOE [28]. Thus, the binary DOE has been developed into a useful and versatile tool in modern optical research.

As we all know, polarization is one of the most important and intrinsic properties of a beam and can influence the focusing properties directly [29]. Over the past decade the focus shaping of the CV beam has been researched extensively, and great success has been achieved in the generation

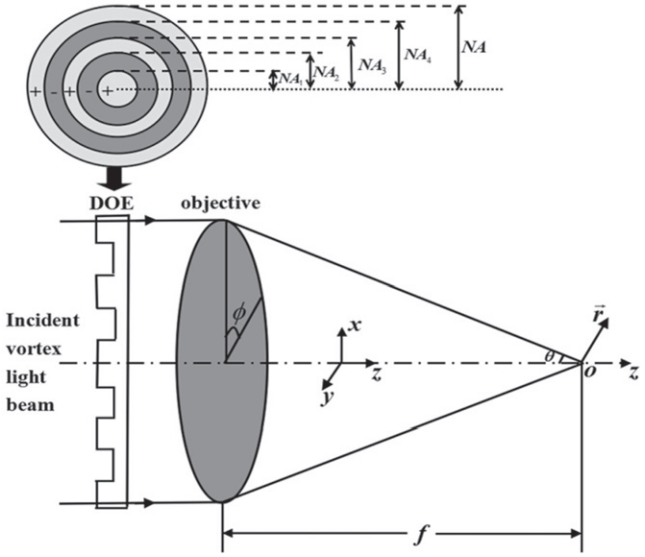

Figure 1. Scheme of the tight focusing system.

of various special beam patterns [18–28]. Recently, circularly polarized vortex beams have attracted a great deal of attention due to their novel properties [30–36]. It is well known that circularly polarized vortex beams carry both spin angular momentum (SAM) and orbital angular momentum (OAM). More interesting, the SAM can be converted into OAM under tightly focused conditions [32]. Up until now, the focusing properties of the circularly polarized vortex beams have been studied [30, 33]. However, to the best of our knowledge, there are no reports on the focus shaping of partially coherent circularly polarized vortex beams. Our aim in this paper is to explore a new 3D focus shaping technique using the combination of partially coherent circularly polarized vortex beams with a binary DOE. Based on the vector diffraction theory [37], we theoretically studied the tight focusing properties of partially coherent circularly polarized vortex beams through a high numerical aperture (NA) lens combined with a binary DOE with five concentric zones. It is found that the focusing properties are largely dependent on the topological charges, beam widths, coherence lengths of the incident beams, and the parameters of the binary DOE. By choosing some suitable values of relevant parameters, we have obtained several interesting and useful beam patterns, such as optical chain, optical needle, optical dark channel, flat-topped field, and 3D optical cage. Furthermore, a new kind of 3D optical cage with a controllable switch has been created by our method. The novel function of this 3D optical cage may find specific application in modern optics, especially for trapping and manipulating particles/atoms in experiment.

2. Theoretical analysis

According to the vector diffraction theory [37], the electric field components near the focus of a circularly polarized beam through a high-NA lens combined with a binary DOE can be written as [33]

$$E(r,\varphi,z)=\begin{bmatrix}E_x\\E_y\\E_z\end{bmatrix}=-\frac{ikf}{2\pi}\int_0^{\alpha}\int_0^{2\pi}A(\theta,\phi)T(\theta)\sin\theta\sqrt{\cos\theta}\times\begin{bmatrix}\cos^2\phi\cos\theta+\sin^2\phi\\ \pm i\cos\phi\sin\phi(\cos\theta-1)\\ \cos\phi\sin\phi(\cos\theta-1)\\ \pm i\left(\cos^2\phi+\sin^2\phi\cos\theta\right)\\ \sin\theta\exp(\pm i\phi)\end{bmatrix}\times\exp[ik(z\cos\theta+r\sin\theta\cos(\phi-\varphi))]\times d\phi d\theta \quad (1)$$

where r, φ, and z are the cylindrical coordinates of an observation point, ϕ is the azimuthal angle of the incident beam, $\alpha=\arcsin\left(NA/n_0\right)$ which represents the maximal value of the convergence angle θ, and $n_0=1$ is the index of refraction of free space. $k=2\pi/\lambda$ is the wave number, f is the focal distance, and $A(\theta,\phi)$ is the pupil apodization function at the objective aperture surface. The schematic of a tightly focused system is shown in figure 1. A binary DOE with five concentric rings is used before the high- NA lens, with the transmission function $T(\theta)$ defined as

$$T(\theta)=\begin{cases}1 & for\ \ 0\leqslant\theta<\alpha_1,\\ & \alpha_2\leqslant\theta<\alpha_3,\ \alpha_4\leqslant\theta\leqslant\alpha\\ -1 & for\ \ \alpha_1\leqslant\theta<\alpha_2,\\ & \alpha_3\leqslant\theta<\alpha_4\end{cases} \quad (2)$$

The four angles α_i $(i=1,...4)$ correspond to angles in the image space for the transition edges of the binary DOE. By using the following coordinate transformations:

$$E_r=E_x\cos\varphi+E_y\sin\varphi$$
$$E_\varphi=-E_x\sin\varphi+E_y\cos\varphi \quad (3)$$

we can derive the field expression in cylindrical coordinates as

$$E(r,\varphi,z)=\begin{bmatrix}E_{\pm,r}\\E_{\pm,\varphi}\\E_{\pm,z}\end{bmatrix}=-\frac{ikf}{2\pi}\int_0^{\alpha}\int_0^{2\pi}A(\theta,\phi)T(\theta)\sin\theta\sqrt{\cos\theta}\times\exp[ik(z\cos\theta+r\sin\theta\cos(\phi-\varphi))]\times\begin{bmatrix}\exp(\pm i\phi)\cos\theta\cos(\phi-\varphi)\\ \mp i\exp(\pm i\phi)\sin(\phi-\varphi)\\ \exp(\pm i\phi)\cos\theta\sin(\phi-\varphi)\\ \pm i\exp(\pm i\phi)\cos(\phi-\varphi)\\ \sin\theta\exp(\pm i\phi)\end{bmatrix}\times d\phi d\theta \quad (4)$$

From the above expression, one can find that the electric field of the r, φ, and z polarized components has two values,

respectively. For simplicity, we define the electric field $E_{+,i}(i = r, \varphi, z)$ as a right-hand circularly (RHC) polarized component and $E_{-,i}(i = r, \varphi, z)$ as a left-hand circularly (LHC) polarized component [32, 33].

Based on the coherence theory, the cross-spectral density matrix of such partially coherent circularly polarized vortex beams in the observed plane can be expressed as [38]

$$\overleftrightarrow{W}(\boldsymbol{r}_1, \boldsymbol{r}_2, z) = \begin{bmatrix} W_{xx}(\boldsymbol{r}_1, \boldsymbol{r}_2, z) & W_{xy}(\boldsymbol{r}_1, \boldsymbol{r}_2, z) & W_{xz}(\boldsymbol{r}_1, \boldsymbol{r}_2, z) \\ W_{yx}(\boldsymbol{r}_1, \boldsymbol{r}_2, z) & W_{yy}(\boldsymbol{r}_1, \boldsymbol{r}_2, z) & W_{yz}(\boldsymbol{r}_1, \boldsymbol{r}_2, z) \\ W_{zx}(\boldsymbol{r}_1, \boldsymbol{r}_2, z) & W_{zy}(\boldsymbol{r}_1, \boldsymbol{r}_2, z) & W_{zz}(\boldsymbol{r}_1, \boldsymbol{r}_2, z) \end{bmatrix} \tag{5}$$

where the element of the matrix is given by

$$W_{jk}(\boldsymbol{r}_1, \boldsymbol{r}_2, z) = \left\langle E_j^*(r_1, \varphi_1, z) E_k(r_2, \varphi_2, z) \right\rangle \quad \text{where } (j, k = x, y, z) \tag{6}$$

Here $\boldsymbol{r}_1$ and $\boldsymbol{r}_2$ are two arbitrary points located in the observed plane. r_1, r_2 and φ_1, φ_2 are the modulus and the angles of the position vectors $\boldsymbol{r}_1$, $\boldsymbol{r}_2$, respectively. The asterisk stands for the complex conjugate, and the angle brackets denote an ensemble average monochromatic realization of the field. By setting $r_1 = r_2 = r$ and $\varphi_1 = \varphi_2 = \varphi$, we can obtain the total intensity distribution in the focal region as follows:

$$I(r, \varphi, z) = W_{xx}(\boldsymbol{r}, \boldsymbol{r}, z) + W_{yy}(\boldsymbol{r}, \boldsymbol{r}, z) + W_{zz}(\boldsymbol{r}, \boldsymbol{r}, z) \tag{7}$$

By using the following coordinate transformations:

$$\begin{aligned} E_x(r, \varphi, z) &= E_r(r, \varphi, z)\cos\varphi - E_\varphi(r, \varphi, z)\sin\varphi \\ E_y(r, \varphi, z) &= E_r(r, \varphi, z)\sin\varphi + E_\varphi(r, \varphi, z)\cos\varphi \end{aligned} \tag{8}$$

the intensity expression in the focal plane with cylindrical coordinates can be derived as

$$I(r, \varphi, z) = W_{rr}(\boldsymbol{r}, \boldsymbol{r}, z) + W_{\varphi\varphi}(\boldsymbol{r}, \boldsymbol{r}, z) + W_{zz}(\boldsymbol{r}, \boldsymbol{r}, z) \tag{9}$$

where

$$W_{jk}(\boldsymbol{r}_1, \boldsymbol{r}_2, z) = \left\langle E_j^*(r_1, \varphi_1, z) E_k(r_2, \varphi_2, z) \right\rangle \quad \text{where } (j, k = r, \varphi, z) \tag{10}$$

In this paper, we assume the field in the source plane is a Laguerre—Gaussian mode field, which can be expressed as [32, 39]

$$A(r, \phi) = E_0 \left(\frac{\sqrt{2}r}{w_0} \right)^{|m|} \exp\left(-\frac{r^2}{w_0^2} \right) \times \exp(im\phi)\exp(i\beta) \tag{11}$$

where E_0 is the characteristic amplitude and w_0 is the beam width in the source plane, m is the topological charge of the vortex beams, and β is an arbitrary phase (as a spatially distributed random variable). For typical objective lenses that obey the sine condition, the ray projection function is given by $r = f\sin\theta$. Thus, the pupil apodization function at the objective aperture surface can be rewritten as [32, 39]

$$A(\theta, \phi) = E_0 \left(\frac{\sqrt{2} f \sin\theta}{w_0} \right)^{|m|} \times \exp\left(-\frac{f^2 \sin^2\theta}{w_0^2} \right) \exp(im\phi)\exp(i\beta) \tag{12}$$

Assuming that the statistical distribution of β corresponds to a Gaussian—Schell correlator, the cross-spectral density of the partially coherent vortex beams at the source plane can be expressed as [39, 40]

$$\begin{aligned} &A^*(\theta_1, \phi_1)A(\theta_2, \phi_2) \\ &= |E_0|^2 \left(\frac{2f^2 \sin\theta_1 \sin\theta_2}{w_0^2} \right)^{|m|} \\ &\times \exp\left[-\frac{f^2 \sin^2\theta_1 + f^2 \sin^2\theta_2}{w_0^2} \right] \\ &\times \exp\left\{ -\left(f^2 \left[\sin^2\theta_1 + \sin^2\theta_2 - 2\sin\theta_1 \times \sin\theta_2 \cos(\phi_1 - \phi_2) \right] / (L_c^2) \right) \right\} \\ &\times \exp\left[im(\phi_2 - \phi_1) \right] \end{aligned} \tag{13}$$

where L_c is the coherence length of the source. On substituting equation (13) into equation (4), and after tedious calculation, the analytical expressions of $W_{rr}(\boldsymbol{r}_1, \boldsymbol{r}_2, z)$ can be expressed as follows:

$$\begin{aligned} &W_{rr}(r_1, r_2, \varphi_1, \varphi_2, z) \\ &= \left(\frac{kf}{2} \right)^2 \sum_{n=-\infty}^{\infty} \int_0^\alpha \int_0^\alpha C^*(\theta_1, z) C(\theta_2, z) J_n(kr_1 \sin\theta_1) \\ &\times \Big\{ \Big[(\cos\theta_2 + 1) J_n(kr_2 \sin\theta_2) \\ &- (\cos\theta_2 - 1) J_{n\mp 2}(kr_2 \sin\theta_2) \Big] \\ &\times \exp\left[\mathrm{i}(n \mp 1)(\varphi_1 - \varphi_2) \right] (\cos\theta_1 + 1) \\ &\times I_{m+n}\left(\frac{2f^2 \sin\theta_1 \sin\theta_2}{L_c^2} \right) \\ &+ \Big[(\cos\theta_2 - 1) J_n(kr_2 \sin\theta_2) \\ &- (\cos\theta_2 + 1) J_{n\pm 2}(kr_2 \sin\theta_2) \Big] \\ &\times \exp\left[\mathrm{i}(n \pm 1)(\varphi_1 - \varphi_2) \right] (\cos\theta_1 - 1) \\ &\times I_{m+n+2}\left(\frac{2f^2 \sin\theta_1 \sin\theta_2}{L_c^2} \right) \Big\} d\theta_1 d\theta_2 \end{aligned} \tag{14}$$

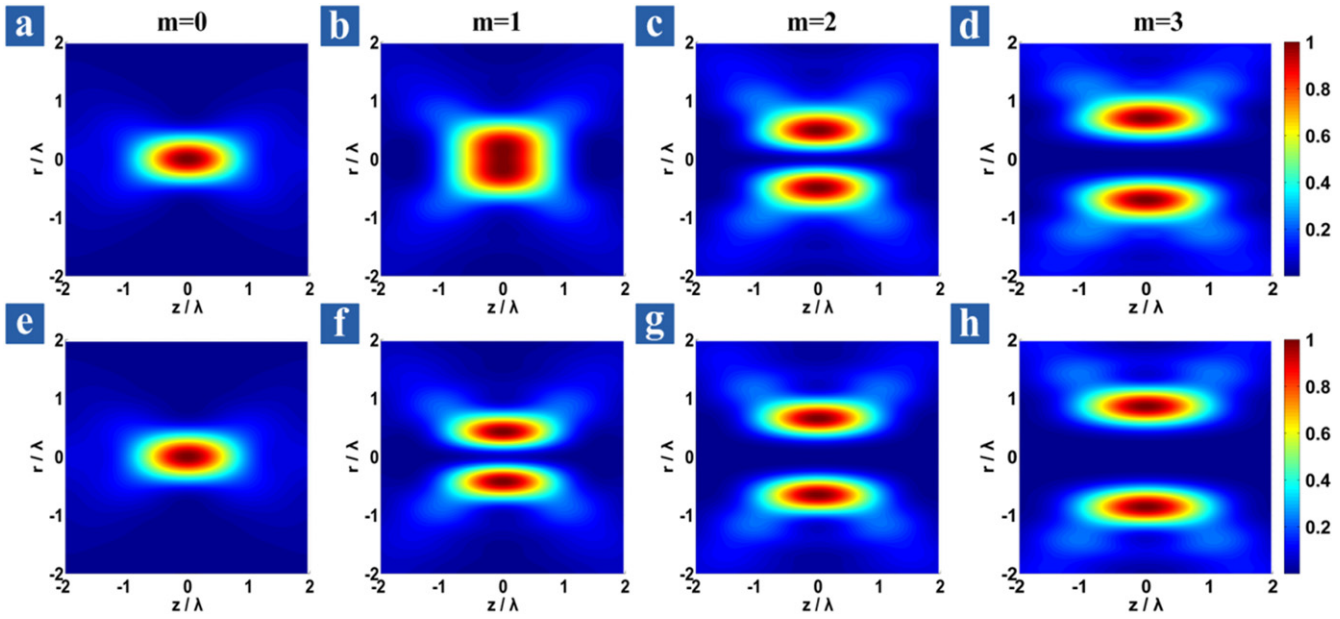

Figure 2. Contour plots for the total intensity distributions in the focal region of the partially coherent circularly polarized vortex beams for different values of topological charge. (a)–(d) LHC polarized vortex beams; (e)–(h) RHC polarized vortex beams. The other parameters are chosen as $\lambda = 633$ nm, $f = 1$ cm, $w_0 = 1$ cm, $L_c = 5$ cm, and $NA = 0.96$.

$$
\begin{aligned}
&W_{\varphi\varphi}(r_1, r_2, \varphi_1, \varphi_2, z) \\
&= \left(\frac{kf}{2}\right)^2 \sum_{n=-\infty}^{\infty} \int_0^{\alpha}\int_0^{\alpha} C^*(\theta_1, z) C(\theta_2, z) J_n(kr_1 \sin\theta_1) \\
&\quad \times \Big\{ \Big[(\cos\theta_2 + 1) J_n(kr_2 \sin\theta_2) \\
&\qquad + (\cos\theta_2 - 1) J_{n\mp 2}(kr_2 \sin\theta_2) \Big] \\
&\quad \times \exp\big[\mathrm{i}(n \mp 1)(\varphi_1 - \varphi_2) \big] (\cos\theta_1 + 1) \\
&\qquad \times I_{m+n}\left(\frac{2f^2 \sin\theta_1 \sin\theta_2}{L_c^2} \right) \\
&\quad + \Big[(\cos\theta_2 - 1) J_n(kr_2 \sin\theta_2) \\
&\qquad + (\cos\theta_2 + 1) J_{n\pm 2}(kr_2 \sin\theta_2) \Big] \\
&\quad \times \exp\big[\mathrm{i}(n \pm 1)(\varphi_1 - \varphi_2) \big] (\cos\theta_1 - 1) \\
&\qquad \times I_{m+n+2}\left(\frac{2f^2 \sin\theta_1 \sin\theta_2}{L_c^2} \right) \Big\} \\
&\quad \times d\theta_1 d\theta_2
\end{aligned}
\tag{15}
$$

$$
\begin{aligned}
&W_{zz}(r_1, r_2, \varphi_1, \varphi_2, z) \\
&= (kf)^2 \sum_{n=-\infty}^{\infty} \int_0^{\alpha}\int_0^{\alpha} C^*(\theta_1, z) C(\theta_2, z) \\
&\quad \times \sin\theta_1 \sin\theta_2 J_n(kr_1 \sin\theta_1) \\
&\quad \times I_{m+n\pm 1}\left(\frac{2f^2 \sin\theta_1 \sin\theta_2}{L_c^2} \right) \\
&\quad \times J_n(kr_2 \sin\theta_2) \\
&\quad \times \exp\big[\mathrm{i}n(\varphi_1 - \varphi_2) \big] d\theta_1 d\theta_2
\end{aligned}
\tag{16}
$$

where $C(\theta_l, z)$ is given by

$$
\begin{aligned}
&C(\theta_l, z) = E_0 T(\theta_l) \sin\theta_l \sqrt{\cos\theta_l} \exp(ikz\cos\theta_l) \\
&\times \left(\frac{\sqrt{2} f \sin\theta_l}{w_0} \right)^{|m|} \exp\left[-\left(\frac{1}{w_0^2} + \frac{1}{L_c^2} \right) f^2 \sin^2\theta_l \right], \qquad (l = 1,\ 2)
\end{aligned}
\tag{17}
$$

3. Results and discussion

3.1. Direct tightly focusing of the partially coherent circularly polarized vortex beams

In this section, we study the focusing properties of partially coherent circularly polarized vortex beams through a high-NA lens without the binary DOE. Figure 2 shows the focal intensity distribution of partially coherent circularly polarized vortex beams with different values of topological charge m, respectively. As we can see, for topological charge $m = 0$ (i.e., non-vortex beams), both the LHC and RHC polarized beams have the same focal intensity distribution with a bright spot. However, for the topological charge $m = 1$, the focal intensity distribution of the LHC polarized vortex beams exhibits a flat-topped spot, while the focal intensity distribution of the RHC polarized vortex beams shows a dark hollow profile (see figures 2(b) and (f)). This can be attributed to the fact that the SAM has been converted into OAM under the tightly focused conditions. For the LHC polarized beams, the original OAM caused by the vortex phase factor can be compensated by the opposite OAM converted from the SAM, which leads to the bright spot in the intensity distribution. But for the RHC polarized beams, the total OAM can be enhanced

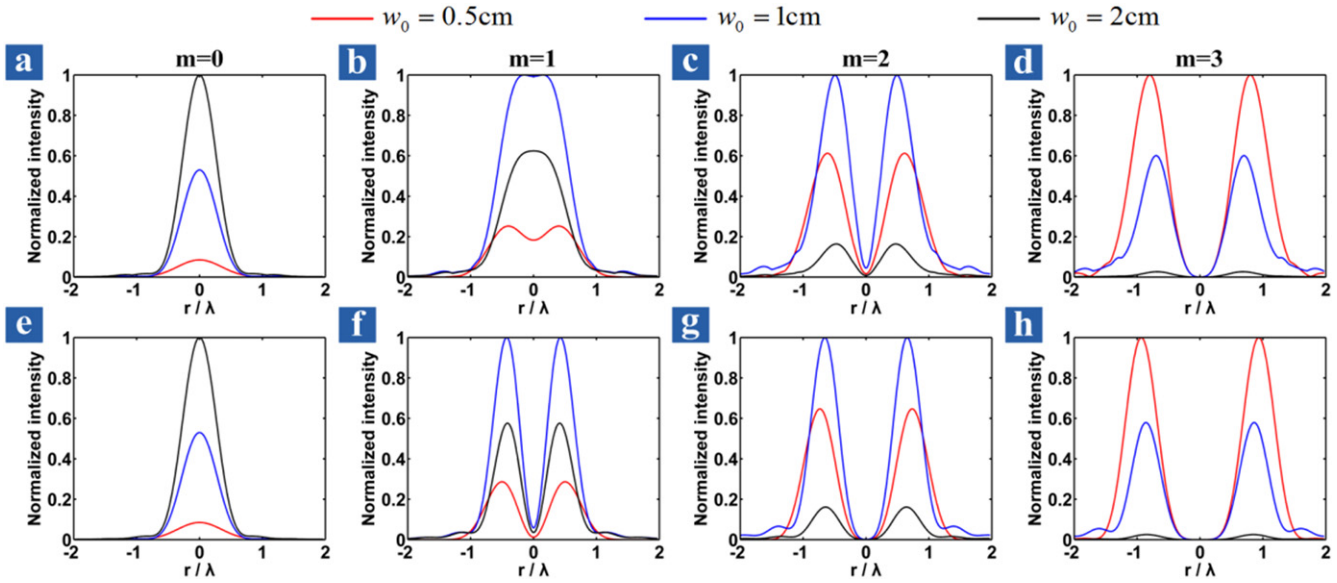

Figure 3. Effect of the beam width w_0 on the focal intensity profiles for partially coherent circularly polarized vortex beams with different values of topological charge. (a)–(d) LHC polarized vortex beams; (e)–(h) RHC polarized vortex beams. The other parameters are the same as in figure 2.

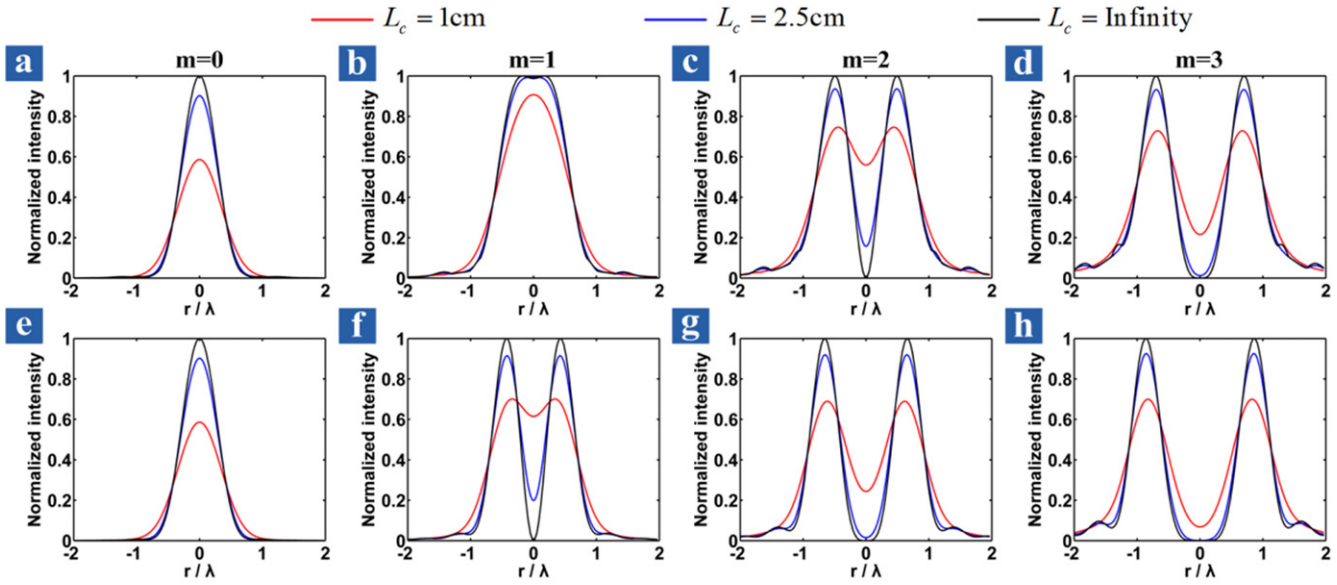

Figure 4. Effect of the coherence length L_c on the focal intensity profiles for partially coherent circularly polarized vortex beams with different values of topological charge. (a)–(d) LHC polarized vortex beams; (e)–(h) RHC polarized vortex beams. The other parameters are the same as in figure 2.

by the OAM converted from the SAM, and thus the intensity distribution forms a doughnut-shaped profile. Our results are in good agreement with those of references [32, 33]. Besides, as the topological charge increases (e.g., $m = 2,3$), the total OAM for both types of beams will be further enhanced, and thus the hollow area of the doughnut shape will be increased.

Figures 3 and 4 show the effects of the beam width w_0 and coherence length L_c on the focal intensity profiles for partially coherent circularly polarized vortex beams with different values of topological charge m, respectively. One can find from figure 3 that when the topological charge $m = 0$ (i.e., non-vortex beams), the focal intensity for both types of beams will be increased as the increment of beam width (see figures 3(a) and (e)). For the topological charge $m = 1,\ 2$, an interesting result can be found: The total intensity for both types of beams is maximal when the beam width $w_0 = 1\ cm$; it indicates that the beam's focusing is the strongest under the condition that the beam width exactly equals the focal length f, which is consistent with the assumption of Shu [40, 41]. However, with the further increase of the topological charge (e.g., $m = 3$), this assumption is not suitable for the circularly polarized vortex beams anymore. The focal intensity for both

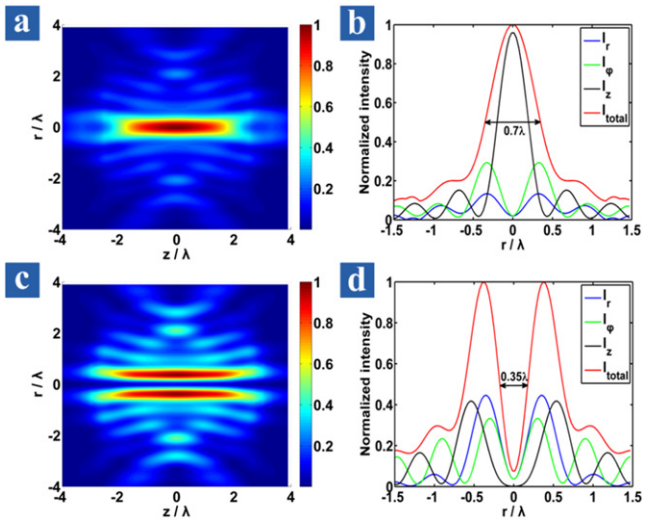

Figure 5. Normalized intensity distributions of the generated optical needle and optical dark channel. (a) and (c) Contour plots for the intensity distribution in the r—z plane; (b) and (d) Normalized intensity profiles at the focal plane.

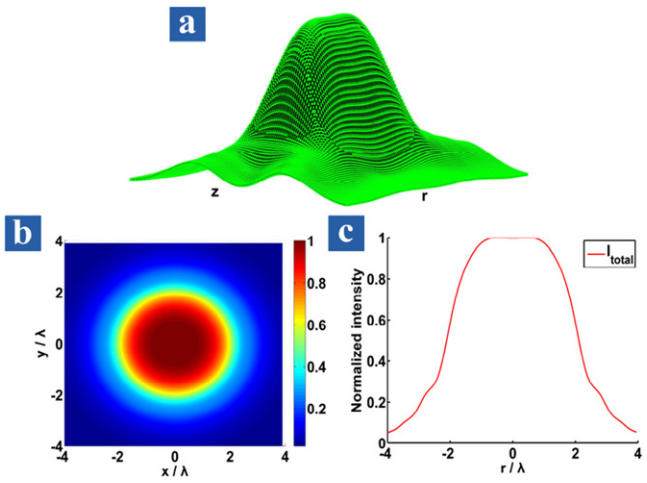

Figure 6. Normalized intensity distribution of the generated flat-topped focal shape. (a) 3D plot of the intensity distribution in the vicinity of the focus; (b) Contour plot for the intensity distribution in the x—y plane; (c) Normalized intensity profile at the focal plane.

types of beams will be decreased with the increase of beam width, which is quite opposite to the case of $m = 0$. From figure 4, one can find that the focal intensity will be increased with the increase of coherence length for both types of beams. Furthermore, one can also find that for a smaller coherence length, the convex or concave of the intensity profile in the focal plane becomes more even. These features may be helpful for shaping the highly focused circularly polarized vortex beams in experiment.

3.2. Focus shaping of partially coherent circularly polarized vortex beams using a binary DOE

In this section, some numerical results are presented to show the focus shaping of partially coherent circularly polarized

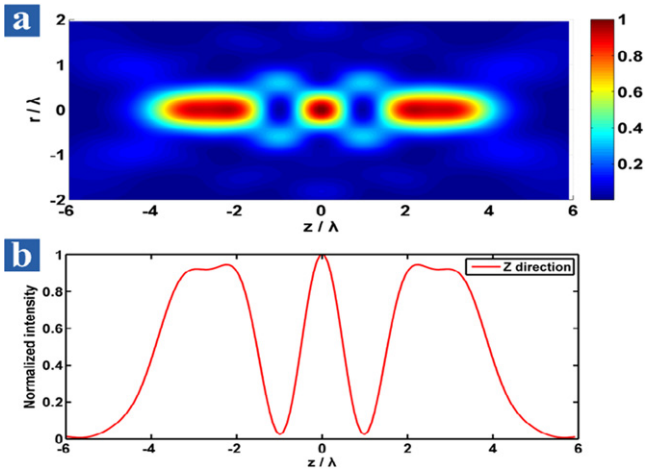

Figure 7. Normalized intensity distribution of the generated optical chain. (a) Contour plot for the intensity distribution in the r—z plane; (b) Normalized intensity profile along the z-direction.

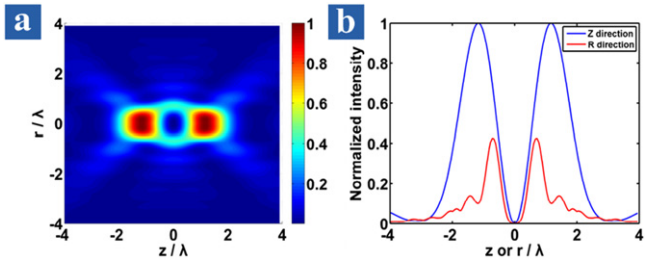

Figure 8. Normalized intensity distribution of the generated optical cage. (a) Contour plot for the intensity distribution in the r—z plane; (b) Normalized intensity profiles in two different directions.

vortex beams through a high-NA lens combined with a binary DOE. One can find from figure 5(a) that an optical needle with a depth of focus (DOF) of about 3λ can be generated by the partially coherent LHC polarized vortex beams through the hybrid lens. The radial component I_r, azimuthal component I_φ, and longitudinal component I_z of the optical needle are also plotted in figure 5(b), respectively. It can be seen clearly that the longitudinal component plays a dominant role in the total intensity, and a sub-wavelength spot with a full width at half maximum of about 0.7λ can be formed at the focal plane. In addition, one can also find from figure 5(c) that an optical dark channel with a dark core of about 0.35λ and a DOF of about 5λ can be obtained by the partially coherent RHC polarized vortex beams with the hybrid lens under the same conditions. The three polarized components are also plotted in figure 5(d). Here the parameters are chosen as $\alpha_1 = 9.46°$, $\alpha_2 = 21.79°$, $\alpha_3 = 34.25°$, $\alpha_4 = 46.87°$, $NA = 0.96$ for the binary DOE, and $m = 1$, $w_0 = 1$ cm, $L_c = 5$ cm for the beams.

As indicated by figure 6, a flat-topped intensity distribution at the focal plane can be formed for the partially coherent RHC polarized vortex beams by choosing suitable values of topological charge, coherence length, and some suitable parameters of the binary DOE. The diameter of the

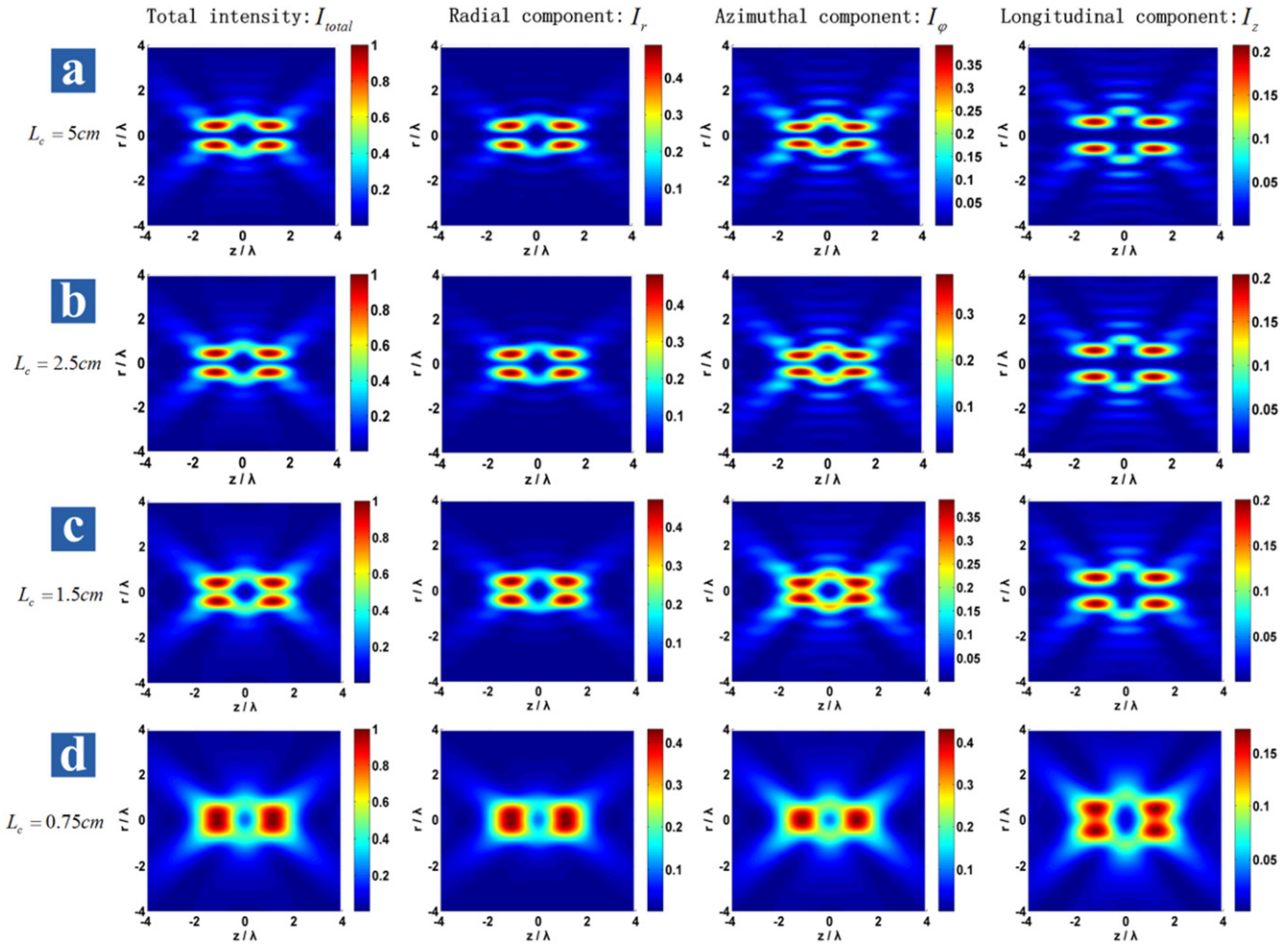

Figure 9. Contour plots for the generated 3D optical cages and the three polarized components for different values of the coherence length of the incident beams. (a) $L_c = 5$ cm; (b) $L_c = 2.5$ cm; (c) $L_c = 1.5$ cm; (d) $L_c = 0.75$ cm.

uniform light spot is about 2λ. Here the parameters are chosen as $m = 5$, $w_0 = 1$ cm, $L_c = 0.25$ cm for the beams, and $\alpha_1 = 9.46°$, $\alpha_2 = 20.79°$, $\alpha_3 = 34.25°$, $\alpha_4 = 46.87°$, $NA = 0.98$ for the binary DOE.

Figure 7 shows that a short optical chain that contains two dark optical cage areas can be generated by the partially coherent LHC polarized beams through the hybrid lens. To achieve this special distribution, the parameters are chosen as $m = 0$, $w_0 = 1$ cm, $L_c = 5$ cm for the beams, and $\alpha_1 = 3.48°$, $\alpha_2 = 4.77°$, $\alpha_3 = 33.36°$, $\alpha_4 = 46°$, $NA = 0.96$ for the binary DOE. Figure 8 shows an ordinary 3D optical cage generated by the tightly focused partially coherent LHC polarized vortex beams through the binary DOE. One can find from figure 8(a) that the optical cage has an ellipsoid dark area surrounded by regions of higher intensity. Figure 8(b) plots the intensity profiles along the radial (red line) and axial (blue line) directions, respectively. In order to achieve this optical cage, we choose the parameters as $m = 1$, $w_0 = 1$ cm, $L_c = 5$ cm for the beams, and $\alpha_1 = 4.46°$, $\alpha_2 = 15.79°$, $\alpha_3 = 17.25°$, $\alpha_4 = 52.37°$, $NA = 0.96$ for the binary DOE.

3.3. Generation of a 3D optical cage with a controllable switch

In this section, we show the generation of a 3D optical cage with a controllable switch by using the partially coherent RHC polarized vortex beams. It is well known that the 3D optical cage can be employed as optical tweezers for trapping low-refractive-index or light-absorbing particles, and the optical dark channel can be used as a pipeline for transporting these particles. If the interconversion between the 3D optical cage and the optical dark channel (i.e., creating a 3D optical cage with a controllable switch) can be realized while only changing one parameter of the incident beams, we can foresee that these particles can be more conveniently and effectively manipulated in experiment, which may open a new way to improve the non-contact manipulation capability of micrometer-sized particles.

Figure 9 shows the focal intensity distributions of the partially coherent RHC polarized vortex beams through the hybrid lens for different values of the coherence length $L_c$of the incident beams, respectively. One can find that with the decrease of the coherence length, the initial 'open' state for the optical cage gradually evolves into a final 'closed' state,

and the dark area of the optical cage decreases simultaneously. The three polarized components I_r, I_φ, and I_z are also plotted in figure 9. In experiment, it is convenient to control the coherence length of the incident beams by using a rotating ground-glass disk [42–44]. Thus, we can expect that such a 3D optical cage with a controllable switch can be realized by using this method. In order to create this 3D optical cage with a controllable switch, we choose the parameters as $m = 1$ and $w_0 = 1$ cm for the beams, and $\alpha_1 = 4.46°$, $\alpha_2 = 15.79°$, $\alpha_3 = 17.25°$, $\alpha_4 = 52.37°$, $NA = 0.96$ for the binary DOE.

4. Conclusions

In summary, we have proposed a 3D focus shaping technique by focusing partially coherent circularly polarized vortex beams using a binary DOE and a high- NA lens. The key optical element in the whole setup is the binary DOE with five concentric zones, which could provide an added degree of freedom for shaping the focal distribution. By appropriately adjusting the parameters of the incident beams, numerical aperture of the objective lens, and the design of the binary DOE, the intensity distribution in the vicinity of the focus can be tailored in three dimensions, and thus the purpose of the focus shaping can be achieved. Numerical results show that the partially coherent circularly polarized vortex beams can be used to generate several special beam patterns. Furthermore, the suggested method successfully creates a 3D optical cage with a controllable switch. Our work may find valuable application in optical tweezers, microscopes, laser processing, and so on.

Note that recent methods for generation of a 3D optical cage have been suggested both theoretically [12, 19, 22, 26, 28] and experimentally [2, 4, 7]. Now we can see that the formation of a 3D optical cage is also possible with the usage of circularly polarized vortex beams. Controlling the switch of the 3D optical cage may provide a novel way for trapping and manipulating particles/atoms.

Acknowledgments

This work is supported by the National Natural Science Foundation of China (NSFC) under Grants Nos. 21133008 and 11374015. Acknowledgment is also given to the Thousand Youth Talents Plan and 'Interdisciplinary and Cooperative Team' of CAS.

References

[1] Arlt J and Padgett M 2000 *Opt. Lett.* **25** 191
[2] Tai P, Hsieh W and Chen C 2004 *Opt. Express.* **12** 5827
[3] Zhao Y, Zhan Q, Zhang Y and Li Y 2005 *Opt. Lett.* **30** 848
[4] Chen Y and Cai Y 2014 *Opt. Lett.* **39** 2549
[5] Wang F and Cai Y 2008 *Opt. Lett.* **33** 1795
[6] Cai Y and Lin Q 2003 *Opt. Commun.* **215** 239
[7] Yelin D, Bouma B E and Tearney G J 2004 *Opt. Lett.* **29** 661
[8] Bokor N and Davidson N 2006 *Opt. Lett.* **31** 149
[9] Hu K, Chen Z and Pu J 2012 *Opt. Lett.* **37** 3303
[10] Nie Z, Shi G, Zhang X, Wang Y and Song Y 2014 *Opt. Commun.* **331** 87
[11] Guo L, Tang Z, Liang C and Tan Z 2011 *Opt. Laser Technol.* **43** 895
[12] Kozawa Y and Sato S 2006 *Opt. Lett.* **31** 820
[13] Lin J, Ma Y, Jin P, Davies G and Tan J 2013 *Opt. Express.* **21** 13193
[14] McGloin D, Spalding G, Melville H, Sibbett W and Dholakia K 2003 *Opt. Commun.* **225** 215
[15] Bokor N and Davidson N 2007 *Opt. Commun.* **270** 145
[16] Li J, Lu T and Guo L 2012 *Opt. Laser. Eng.* **50** 996
[17] Török P and Munro P 2004 *Opt. Express.* **12** 3605
[18] Yang L, Xie X, Wang S and Zhou J 2013 *Opt. Lett.* **38** 1331
[19] Bokor N and Davidson N 2007 *Opt. Commun.* **279** 229
[20] Nie Z, Li Z, Shi G, Zhang X, Wang Y and Song Y 2014 *Opt. Laser. Eng.* **59** 93
[21] Chen H, Tripathi S and Toussaint K C 2014 *Opt. Lett.* **39** 834
[22] Wang X, Ding J, Qin J, Chen J, Fan Y and Wang H 2009 *Opt. Commun.* **282** 3421
[23] Zhan Q and Leger J 2002 *Opt. Express.* **10** 324
[24] Lin J, Yin K, Li Y and Tan J 2011 *Opt. Lett.* **36** 1185
[25] Kitamura K, Sakai K and Noda S 2010 *Opt. Express.* **18** 4518
[26] Chen W and Zhan Q 2006 *Opt. Commun.* **265** 411
[27] Wang H, Shi L, Lukyanchuk B, Sheppard C and Chong C T 2008 *Nat. Photon.* **2** 501
[28] Weng X, Gao X, Guo H and Zhuang S 2014 *Appl. Opt.* **53** 2470
[29] Zhan Q 2009 *Adv. Opt. Photon.* **1** 1
[30] Zhan Q 2006 *Opt. Lett.* **31** 867
[31] Moh K, Yuan X, Bu J, Burge R and Gao B Z 2007 *Appl. Opt.* **46** 7544
[32] Zhao Y, Edgar J, Jeffries G, McGloin D and Chiu D 2007 *Phys. Rev. Lett.* **99** 073901
[33] Chen B, Zhang Z and Pu J 2009 *J. Opt. Soc. Am.* A **26** 862
[34] Yang S, Powers P and Zhan Q 2009 *Opt. Commun.* **282** 4657
[35] Neugebauer M, Banzer P, Bauer T, Orlov S, Lindlein N, Aiello A and Leuchs G 2014 *Phys. Rev.* A **89** 013840
[36] Chen J, Gao X, Zhu L, Xu Q and Ma W 2014 *Opt. Commun.* **318** 100
[37] Richards B and Wolf E 1959 *Proc. R. Soc. London, Ser.* A **253** 358
[38] Lindfors K, Setälä T, Kaivola M and Friberg A 2005 *J. Opt. Soc. Am.* A **22** 561
[39] Shu J, Chen Z, Pu J, Zhu J and Liu D A 2013 *Opt. Commun.* **295** 5
[40] Shu J, Chen Z and Pu J 2013 *J. Opt. Soc. Am.* A **30** 916
[41] Shu J, Liu Y, Chen Z and Pu J 2014 *J. Mod. Opt.* **61** 954
[42] Zhao C, Dong Y, Wang Y, Wang F, Zhang Y and Cai Y 2012 *Appl. Phys.* B **109** 345
[43] Wang F, Liu X, Yuan Y and Cai Y 2013 *Opt. Lett.* **38** 1814
[44] Cai Y, Chen Y and Wang F 2014 *J. Opt. Soc. Am.* A **9** 2083